Monitoring of the Ground Subsidence in Macao Using the PSI Technique

Shaojing Jiang[1(✉)], Fenghua Shi[2], Bo Hu[3], Weibo Wang[1],
and Qianguo Lin[4]

[1] Research Institute of Yanchang Petroleum (GROUP) Co., Ltd,
Xi'an 710075, China
`jshj70l0@sina.com, ffslxf@l63.com,`
`wangweibol63@l63.com`
[2] Urban and Rural Construction Institute, Hebei Agricultural University,
Baoding 071000, China
`shifenghual98l@l63.com`
[3] Department of Surveying and Mapping,
Guangdong University of Technology, Guangzhou 510006, China
`358863955@qq.com`
[4] Carbon Capture and Storage (Beijing) Technology Co. Ltd,
Beijing 100089, China
`lilinshi@hotmail.com`

Abstract. In this paper, we investigated the long-term reclamation-induced ground subsidence in Macao, a coastal city of southern China. Persistent Scatterers Interferometry (PSI) technique was applied to retrieve the deformation rate in Macao during the period from April 2003 to August 2010 with a total of 41 scenes of descending ASAR data sets. The PSI-retrieved results showed a relatively stable pattern in Macao Peninsula, Taipa Island and Coloane Island, with an average subsidence velocity of -3 mm/y. In contrast, relatively large subsidence rates were highlighted in Cotai area, a newly reclamation land in 1990s, in which an average subsidence velocity was about -10 mm/y. A consistent relationship between the PSI results and the leveling measurements indicated that this PSI technique is an effective tool to monitor the reclamation-induced ground subsidence with a high accuracy and adequate spatial details. Accordingly the valuable ground subsidence results generated by PSI can be used not only for early detection and remedial activities of potential settlement of buildings, but also for helping the local government to formulate regional sustainable development planning and decision-making in disaster prevention and mitigation.

Keywords: Persistent Scatterers Interferometry (PSI) · Macao
Reclamation land · Ground subsidence

1 Introduction

Land reclamation from sea is regarded as the most common way to resolve the limited land resource in coastal areas of many countries, including China, Japan, Korea and so on [1–5]. Ground subsidence has been a significant geohazard in reclaimed areas, with

probably large areas of unconsolidated ground material. In particular, the settlement variability is crucial to performance assessment of the reclamation development because this differential settlement can lead to damage of ground constructions and underground facilities.

In recent years, The Differential Interferometry Synthetic Aperture Radar (DInSAR) technique has been proven as an powerful remote sensing tool to map ground tiny deformation, such as volcano dynamics [6, 7], earthquakes [8, 9], groundwater over-exploitation [10, 11], mining [12, 13], coastland reclamation [4, 14–16]. However, this DInSAR technique is limited by the intrinsic problems of temporal and geometrical décor relation as well as atmospheric disturbances [17]. The PSI is a newly developed surface displacement observation technique based on using of a large data set of SAR images over the same area to overcome the limitations of conventional DInSAR, which was first proposed by Ferretti and has been further developed and applied recently [18]. A large number of research projects and applications have demonstrated the remarkable capacity of the PSI technique to detect tiny ground deformation in the literature [19–21]. Particularly in urban areas, for instance that the reclamation-induced ground subsidence [1, 15]. Nevertheless, it is still a challenge to monitor such reclamation settlement due to the complex deformation mechanism relevant to underlying geological conditions and building foundation types.

In this study, we have investigated the surface deformation induced by land reclamation in Macao Special Administrative Region (Macao), a coastal city of China, mostly extended by reclamation since the 17th century. Until now, approximately more than half of the urban area has been built on such reclaimed land and has potential problems of land subsidence. The PSI technique was applied to monitor the reclaimed land deformation based on 41 ASAR images acquired between April 2003 and August 2010. The PSI-retrieved average deformation rates validated by the leveling measurements provided by the Macao Government Cartography and Cadastre Bureau (DSCC) of the Macao, showed that there were significant settlement in reclamation land, especially the new reclamation such as the Cotai area.

2   Study Area and Data Sets

Macao is located in South China, on the western side of the Pearl River Delta as depicted in Fig. 1. It comprises four parts: the Macao Peninsula, the islands of Coloane and Taipa and a newly reclaimed area known as Cotai (Coloane–Taipa). Since Macao has been restricted for the scarce land resource, land reclamation has been a common way to meet the land use demand for growing population and rapid industrial development. Land reclamation from the sea expanded the terrestrial area of the Macao nearly three times, from 11.6 square kilometers in 1912 to 29.9 square kilometers in 2011. The reclaimed land was generally used for commercial, port supporting facilities or simply as landfill sites and residential areas, and approximately half of the urban area in Macao were built on such reclaimed land. The latest large-scale reclamation in Macao has mainly been conducted in the Cotai region since the 1990s. It created a 5.2 square kilometers newly reclaimed land between Taipa and Coloane islands in order to provide a new gambling and tourism area. Numerous large-scale urban
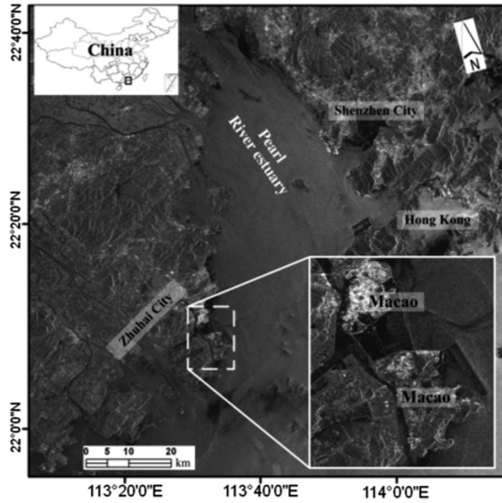
Fig. 1. The geographic location of the study area.

developments have been conducted in the Cotaireclamation area, including the Macao University of Science and Technology, Macao East Asian Games Dome, Cotai Strip, Galaxy World Resort and so on [14]. In solving a scarcity of land at the same time, it brings some related geological problems, causing severe differential ground subsidence in reclamation land.

In the case study, a total of 41 C-band ENVISAT/ASAR scenes over the Macao area were used, acquired between April 2003 and August 2010. Gamma software was employed to process the raw SAR data and interferometric procedure, and IPTA package was used to perform PSI analysis. The ASAR scene on Sep.21, 2008 was used as the master image and 40 interferograms were generated from Single Look Complex (SLC) images. The spatial and temporal baselines of these interferograms are shown in Figs. 2 and 3. The longest spatial baseline is 815 m and the longest temporal baseline is 5.4 years.
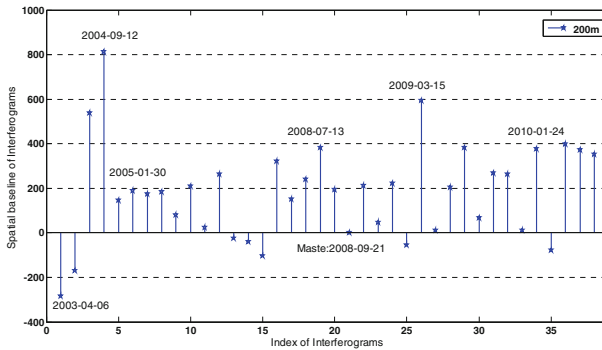

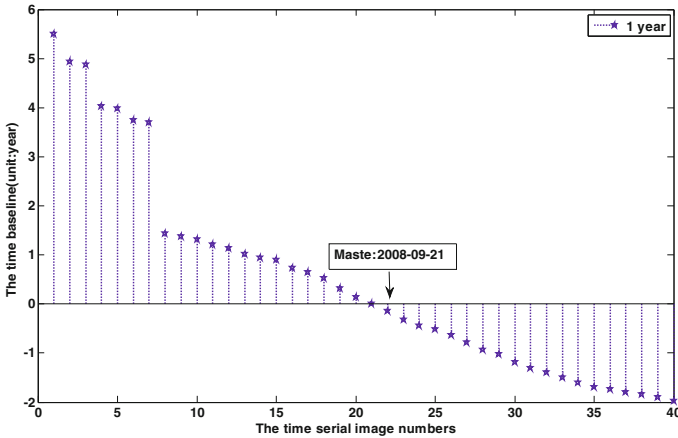**Fig. 2.** Spatial baselines of interferograms.

Fig. 3. Temporal baselines of interferograms.

Besides the SAR datasets, a Digital Elevation Model (DEM) data of the study area with a regular grid spacing of 5 m was used to simulate and remove phase component contributed by topography.

3 Methodology

The Persistent Scatterer Interferometry (PSI) is a powerful remote sensing technique able to measure and monitor displacements of the Earth surface over time. Specifically, PSI is a radar-based technique that belongs to the group of differential interferometric Synthetic Aperture Radar (SAR). The PSI technique is quite different from the traditional DInSAR technique. The key steps for the PSI data processing mainly contain the following steps: selection of common master image, identification and selection of Persistent Scatterers (PS) points, formation of differential interferogram, preliminary estimation of the subsidence velocity and the DEM errors, atmospheric phase removing, final estimation of the subsidence velocity and the DEM errors. Accordingly, we focused on the following processing steps in order to monitor and asses the land subsidence in the reclaimed coastal areas of Macao.

3.1 PS Identification

PS identification is one of the key steps for the PSI processing and analysis. Currently there are three available PS detection methods, so-called coherence coefficient threshold, amplitude dispersion threshold and phase deviation threshold respectively [18]. All the above PS detection methods are single threshold detection, which only emphasized some one aspect characteristic of PS. Therefore it's very easy to errors in PS identification. For instance, coherence coefficient threshold is only considering strong scattering characteristics of the PS but ignoring its stability. The amplitude dispersion threshold and the phase deviation threshold only consider properties of PS

stability while ignoring the strong scattering properties. In view of the shortcomings of the aforementioned PS selection methods, we proposed in this paper an improved method named three-threshold PS detection method based on the average coherence, amplitude, amplitude dispersion information. This method firstly utilized the PS high SNR echo signals characteristic, combination an average of coherence with amplitude threshold select PS candidates (PSCs), and then considering the stability of PS, further selection of the PS from PSC by the amplitude dispersion threshold. The proposed three-threshold PS detection algorithm details as following:

(1) If M + 1 SLC images are resampled to a common master image, one can make M interferograms. According to coherence coefficient formula, calculate the time series coherence coefficient (γ) of each pixel, so each pixel is to form a coherent factor sequence, the coherence coefficient is defined as

$$\gamma = \frac{\left| \sum_{i=1}^{m} \sum_{j=1}^{n} M(i,j) S^*(i,j) \right|}{\sqrt{\sum_{i=1}^{m} \sum_{j=1}^{n} |M(i,j)|^2 \sum_{i=1}^{m} \sum_{j=1}^{n} |S(i,j)|^2}} \quad (1)$$

where M and S are the master and the slave images, S*is the conjugate of slave images, m is the number of rows, n is the number of columns.

(2) Calculate the average coherence of pixel ($\bar{\gamma}$)) in the time series.

$$\bar{\gamma} = \frac{\sum_{m=1}^{M} \gamma_m}{M} \quad (2)$$

(3) According to the experience, set the coherence threshold (about 0.15–0.25), mainy to filter out water and vegetation areas;

(4) Calculate the time serial amplitude value (mA).

(5) Set the amplitude threshold (TA).

$$T_A = \min \left\{ \frac{1}{mn} \sum_{i=1}^{m} \sum_{i=1}^{n} T_{i,j} \right\} \quad (3)$$

where $T_{i,j}$ is the amplitude threshold of i rows and j columns.

(6) Distinguish the PSC, When the correlation coefficient to meet the threshold condition MA>TA, for the PSC points, or non-PSC points.

(7) Calculate the time series standard deviation of the amplitude (σ_A).

(8) Calculate the PSC amplitude dispersion index (D_A).

$$D_A = \frac{\sigma_A}{m_A} \quad (4)$$

(9) Distinguish the PS, set a reasonable threshold, if meet the condition $D_A \leq T_d$, as PS, or non-PS.

In order to verify the validity of the three-threshold PS detection method, we selected the PS using the aforementioned PS selection methods and the three-threshold respectively. Fig. 4(a) shows the coherence coefficient threshold extracted PS, from the view of PS location distribution, most of the extracted PS points connect into the area, only a few PS points appear alone, we can also find that there are some points in Macao sea. Apparently these points are not the true PS points. Therefore, coherence coefficient threshold method is simple in principle and calculation, but this method still has some shortcomings. Fig. 4(b) shows the amplitude dispersion threshold method extracted PS, the extracted PS points are almost all independent, mostly corresponding to hard targets on the ground, we can also easily observe that many hard targets on the ground were not chosen as PS points, but in fact those hard targets are almost PS points. In addition, some non-PS points were wrongly chosen as PS points, this is because the method only considered the PS stable scattering property, while ignoring the PS strong scattering property, it's very easy to cause wrong justice. Fig. 4(c) shows the three-threshold PS detection method extracted PS, the extracted PS are almost all independent distributed in built-up areas, in line with our actual situation. It was proved that the proposed new method is effective and reliable.
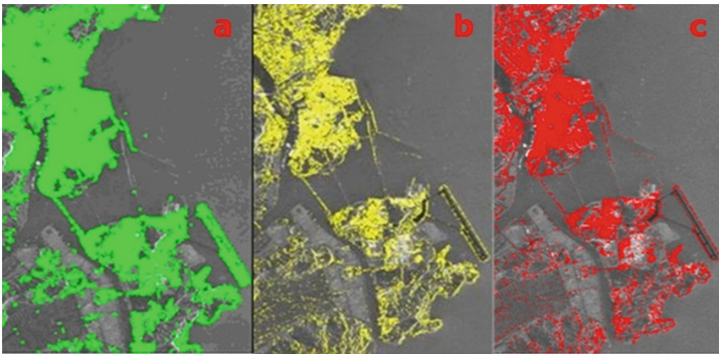
Fig. 4. (a) The coherence coefficient threshold extracted PS. (b) The amplitude dispersion threshold extracted PS. (c) The three-threshold detection method extracted PS

3.2 Differential Interferogram Formation

With $M + 1$ SAR images, precise orbit data and a DEM data, we can obtain differential interferograms with respect to the same master image. For a PS (x) in the interferogram with the temporal baseline of, the differential phase can be written as

$$\Phi(x, t_i) = \phi_{topo}(x, t_i) + \phi_{defo}(x, t_i) + \phi_{atmo}(x, t_i) + \phi_{noise}(x, t_i)$$
$$i = 1 \cdots N \tag{5}$$

where $\phi_{topo}(x, t_i)$ is the phase caused by DEM error, $\phi_{defo}(x, t_i)$ is the phase due to displacement of the point, $\phi_{atmo}(x, t_i)$ is the phase raised by atmospheric delay,

$\phi_{noise}(x, t_i)$ is the decorrelation noise, N is the total number of PS, the topographic phase is a linear function of the perpendicular baseline.

$$\phi_{topo}(x, t_i) = \mu(x, t_i) \cdot \Delta h_x \tag{6}$$

Where $\mu(x, t_i)$ is the height-to-phase conversion factor, and Δh_x is the DEM error at the point. Regarding the deformation phase, it can be separated into two terms, i.e.,

$$\phi_{defo}(x, t_i) = \frac{4\pi}{\lambda} \cdot v(x) \cdot t_i + \phi_{non-linear}(x, t_i) \tag{7}$$

where $v(x)$ is the mean deformation rate of target x, λ is the wavelength of the radar signal, and $\phi_{non-linear}(x, t_i)$ is the phase component due to non-linear motion. The interferometric phase at point can be finally written as

$$\begin{aligned} \Phi(x, t_i) = \mu(x, t_i) \cdot \Delta h_x + \frac{4\pi}{\lambda} \cdot v(x) \cdot t_i + \omega(x, t_i) \\ i = 1 \cdots N \end{aligned} \tag{8}$$

where $\omega(x, t_i)$ is the phase sum of three contributions caused by atmospheric delay, noise and non-linear motion respectively. Considering two neighboring PS point, the phase difference between them can be expressed as

$$\Phi(x, y, t_i) = \mu(x, t_i) \cdot \Delta h_{x,y} + \frac{4\pi}{\lambda} \cdot \Delta v(x, y) \cdot t_i + \Delta \omega_i \tag{9}$$

Where is the difference of DEM errors at these two points, is the velocity difference. is the difference of residual phase, which is assumed to be small, since all its components (i.e., atmospheric difference signal, non-linear deformation and random noise) are small.

3.3   Preliminary Estimation of the Subsidence Velocity and the DEM Errors

In PSI technique the estimation of the subsidence velocity and the DEM errors from the observed wrapped phase pairs are performed by a search through the solution space. Under the condition.

$$|\Delta \omega_i| < \pi \tag{10}$$

The absolute value of the complex ensemble coherence $\hat{\gamma}_{x,y}$ can be adopted as a reliable norm.

$$\hat{\gamma}_{x,y} = \left| \frac{1}{N} \sum_{i=1}^{N} e^{i\Delta\omega_i} \right| \tag{11}$$

The value of coherence lies in the interval [0, 1]. High values imply a good estimation of the velocity difference and the difference of DEM errors. In practice the maximum of coherence is found by sampling two-dimensional solution space with a certain resolution and up to certain bounds, each time evaluating the norm.

After obtaining all maximum values of coherence, we need a threshold to remove the unreliable arcs. Unfortunately the determination of this threshold is not practically straightforward. In other words, users have to select the threshold based on experience. As a reference, the value of 0.75 was used in [19], The parameters (the mean deformation rate and the DEM error) at PS points can then be obtained by integrating the rate differences and the DEM error between all pairs of PS points with respect to a reference point.

3.4 Atmospheric Phase Removing and the Final Estimation of the Parameters

After removing the phase components contributed by linear motion and DEM error on arcs, the residual phase at the PS points can be unwrapped by a weighted least-squares integration. The residual phase contains the components due to, atmospheric delay and random noise. Under the assumption that the atmospheric signal behaves randomly in time and is correlated in space, it can be isolated from other components by low-pass filtering in the spatial domain and high-pass filtering in the temporal domain.

3.5 Final Estimation of the Subsidence Velocity and the DEM Errors

After the estimation of atmospheric phase at PS points, the atmospheric component can be determined by Kriging interpolation, which is referred to as "atmospheric phase screen" (APS). From the differential interferograms without APS, the DEM errors and displacement can be estimated on a pixel by pixel basis. The time series deformation can be estimated by the low-pass temporal filtering mentioned earlier.

4 Results and Discussions

A total of 32600 PS points were detected when the ensemble phase coherence threshold was set to be 0.75, which corresponds approximately to 958 PS points per square kilometer. The distribution of the PS points and the corresponding deformation velocity are shown in Fig. 5. Most of the PS points were identified on the ground buildings in the three original islands of Macao, Taipa and Coloane. The surface deformation rates are relatively low, the average subsidence velocity is about -3 mm/y. It can be explained by the interpretation that the geological conditions of the three original islands are dominated by bedrock of fine-grained and fine-to medium-grained granite. In contrast, the relatively strong ground deformation patterns can be observed in the newly reclamation Cotai, the mean deformation velocity is about -10 mm/y. In addition, the differential deformation over a short distance can be found in Cotai area. This differential settlement might be related to numerous large-scale civil constructions, such as the Macao University of Science and Technology, Cotai Strip, Galaxy World
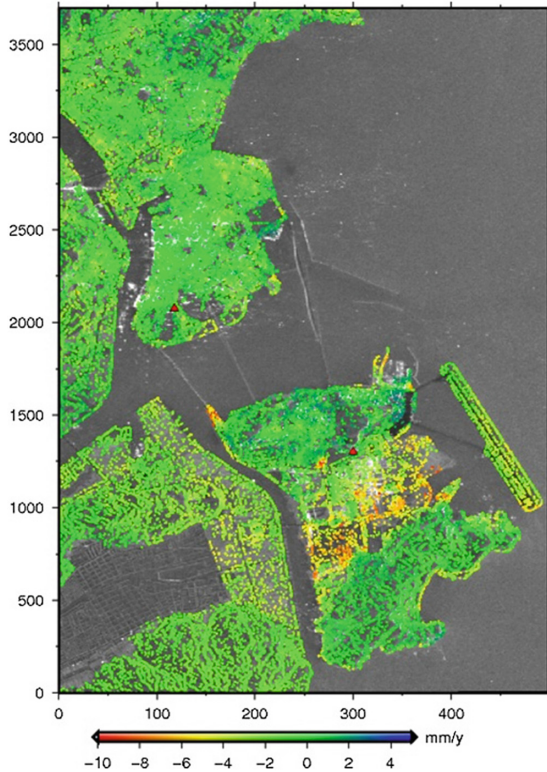
Fig. 5. The deformation rate map estimated by PSI, the redtriangle indicate the ground leveling sites as reference points.

Resort, Macao East Asian Games Dome and so on. Moreover, continuous reclamation of adjacent areas, sand-dominant reclamation material and subterranean structures can result in the differential settlements. The more detailed causes of anomalous phenomenon have still to be investigated by geological engineers.

In order to assess the PSI-obtained results in this study, we conducted a comparison of the PSI deformation velocity with the leveling measurements based on 38 leveling sites provided by DSCC. To enable the comparison, firstly we estimated the mean deformation rates for these sites in the radar line of the sight (LOS) direction based on the leveling measurements by a factor 0.92. Secondly, the location of leveling site is usually not the same as that of the PS, so we searched the PS point nearest from each leveling site and then compared their deformation velocities. The compared results are shown in Fig. 6. For the PSI solution, the PS points G4 and G19 nearest to the corresponding leveling sites were taken as the reference points. The mean values of the velocity difference and the standard deviation of the velocity difference are respectively 1.1 mm/y and 1.9 mm/y for the 38 reference leveling sites, indicating that most of the PSI results are consistent with the leveling results. The validation results are
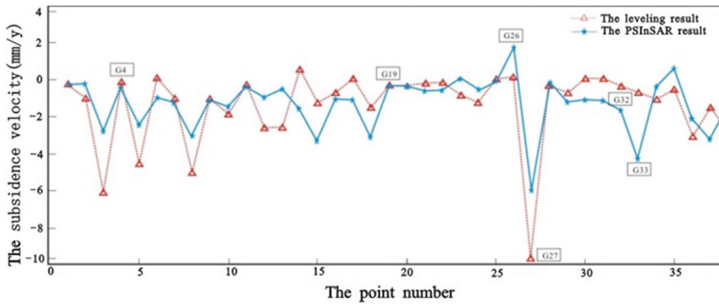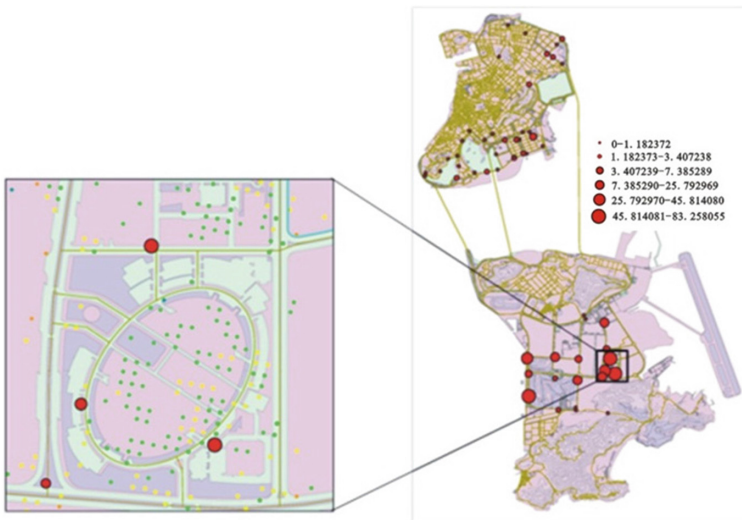
Fig. 6. Comparison between leveling and PSI measurements

comparable with the recent validation experiments available in the scientific literature [14], and demonstrate a reliable achievement in this study.

But large differences do exist at several sites (e.g.G26, G27, G32, G33). The locations of these points are corresponding the Macao East Asian Games Dome in the newly reclaimed Cotaiarea (Fig. 7). The following reasons may be responsible for the large differences between the leveling and the PSI measurements:

(1) The ground deformations are sometimes very localized. The distance between a leveling site and a PS point can cause large difference between the results. For example, the leveling site may measure the ground deformation while InSAR measures the nearby building deformation.

(2) The observation time periods are different between the leveling and the PSI measurements. All of leveling sites with large differences were measured from 2008, much later than some of the SAR data.

Fig. 7. Sites with large differences between leveling and PSI measurements. The size of red circles indicates the magnitude of the differences.

5   Conclusion Remarks

In this paper, the reclamation-induced ground subsidence of Macao was investigated with the PSI technique utilizing the Envisat ASAR data during the period from April 2003 to August 2010. This study has revealed that some parts of the reclaimed area have been experiencing significant land subsidence during the ASAR data acquisition period. The average subsidence rate was approximately -3 mm/y in the islands of Macao, Coloane, Taipa and -10 mm/y in the newly reclaimed land Cotai. The PSI-retrieved results agreed well with the evolution of land reclamation in Macao. A comparison of the results with leveling measurements indicated that the accuracy of the PSI results was around 1.1 mm/y with 90% confidence (2σ) for most of the points.

For monitoring ground deformation in the future in Macao, there are several possible options to improve our understanding the spatial-temporal varieties of reclamation settlements. One is to use high resolution SAR data, e.g., those acquired by TerraSAR, Cosmo-SkyMedand Radarsat-2. Another option is to use the ALOS/PALSAR L-band data characterized by a radar long-wavelength.

References

1. Jiang, L.M., Lin, H.: Integrated analysis of SAR interferometric and geological data for investigating long-term reclamation settlement of Chek Lap Kok Airport, Hong Kong. Eng. Geol. **110**, 77–92 (2010)
2. Kim, J.S., Kim, D.J., Kim, S.W., Won, J.S.: Monitoring of urban land surface subsidence using PSI. Geosci. J. **11**, 59–73 (2007)
3. Kim, J.: Monitoring of surface deformation in urban areas using PSI technique, M. Sc. thesis, Seoul National University, 109 p. (2007)
4. Liu, G., Ding, X.L., Chen, Y.Q., Li, Z.L.: Ground settlement of Chek Lap Kok Airport, Hong Kong, detected by satellite synthetic aperture radar interferometry. Chin. Sci. Bull. **46**(21), 1778–1782 (2001)
5. Stuyfzand, P.J.: The impact of land reclamation on groundwater quality and future drinking water supply in the Netherlands. Water Sci. Technol. **31**, 47–57 (1995)
6. Fernandez, J., Romero, R., Carrasco, D., Tlampo, K.F., Rodriguez-velasco, G., Aparicio, A., Arana, V., Gonzalez-matesanz, F.J.: Detection of displacements on Tenerife Island, Canaries, using radar interferometry. Geophys. J. Int. **160**, 33–45 (2005)
7. Lu, Z., Fatland, R., Wyss, M., Li, S., Eichelberer, J., Dean, K., Freymueller, J.: Deformation of New Trident volcano measured by ERS-1 SAR interferometry, Katmai National Park. Alask. Geophys. Res. Lett. **24**, 695–698 (1997)
8. Flalko, Y., Sandwell, D., Simous, M., Rosen, P.: Three-dimensional deformation caused by the Bam, Iran, earthquake and the origin of shallow slip deficit. Nature **435**, 295–299 (2005)
9. Yen, J.Y., Chen, K.S., Chang, C.P., Boerner, W.M.: Evaluation of earthquake potential and surface deformation by differential interferometry. Remote Sens. Environ. **112**, 782–795 (2008)
10. Bawden, G.W., Thatcher, W., Stein, R.S., Hudnut, K.W., Peltzer, G.: Tectonic contraction across Los Angeles after removal of groundwater pumping effects. Nature **412**, 812–815 (2001)
11. Hoffmann, J.: The future of satellite remote sensing in hydrogeology. Hydrogeol. J. **13**, 247–250 (2005)

12. Herrera, G., Tomas, R., Lopez-sanchez, J.M., Delgado, J., Mallorqui, J.J., Duque, S., Mulas, J.: Advanced DInSAR analysis on mining areas: La Union case study (Murcia, SE Spain). Eng. Geol. **90**, 148–159 (2007)
13. Jung, H.C., Kim, S.W., Jung, H.S., Min, K.D., Won, J.S.: Satellite observation of coal mining subsidence by persistent scatterer analysis. Eng. Geol. **92**, 1–13 (2007)
14. Jiang, L., Lin, H., Cheng, S.: Monitoring and assessing reclamation settlement of coastal areas with advanced InSAR techniques: Macao city (China) case study. Int. J. Remote Sens. **32**, 3565–3588 (2011)
15. Kim, S.W., Lee, C.W., Song, K.Y., Min, K.D., Won, J.S.: Application of L-band differential SAR interferometry to subsidence rate estimation in reclaimed coastal land. Int. J. Remote Sens. **26**, 1363–1381 (2005)
16. Teatini, P., Strozzi, T., Tosi, L., Wegmuller, U., Werner, C., Carbognin, L.: Assessing short- and long-time displacements in the Venice coastland by synthetic aperture radar interferometric point target analysis. J. Geophys. Res. 112, 656–664 (2007)
17. Zebker, H.A., Villasenor, J.: Decorrelation in interferometric radar echoes. IEEE Trans. Geosci. Remote Sens. **30**, 950–959 (1992)
18. Ferretti, A., Prati, C., Rocca, F.: Permanent scatterers in SAR interferometry. IEEE Trans. Geosci. Remote Sens. **39**, 8–20 (2001)
19. Ferretti, A., Prati, C., Rocca, F.: Nonlinear subsidence rate estimation using permanent scatterers in differential SAR interferometry. IEEE Trans. Geosci. Remote Sens. **38**, 2202–2212 (2000)
20. Hu, B., Wang, H.: Monitoring ground subsidence with permanent scatterers interferometry. J. Geodesy Geodyn. **30**, 14–21 (2010)
21. Kampes, B., Hanssen, R.: Ambiguity resolution for permanent scatterer interferometry. IEEE Trans. Geosci. Remote Sens. **42**, 2446–2453 (2004)